

Memcomputing with membrane memcapacitive systems

Y. V. Pershin¹, F. L. Traversa², M. Di Ventra²

¹ Department of Physics and Astronomy, University of South Carolina, Columbia, South Carolina 29208, USA

² Department of Physics, University of California, San Diego, La Jolla, California 92093-0319, USA

E-mail: pershin@physics.sc.edu, ftraversa@physics.ucsd.edu, diventra@physics.ucsd.edu

Abstract. We show theoretically that networks of membrane memcapacitive systems – capacitors with memory made out of membrane materials – can be used to perform a complete set of logic gates in a massively parallel way by simply changing the external input amplitudes, but not the topology of the network. This *polymorphism* is an important characteristic of memcomputing (computing with memories) that closely reproduces one of the main features of the brain. A practical realization of these membrane memcapacitive systems, using, e.g., graphene or other 2D materials, would be a step forward towards a solid-state realization of memcomputing with passive devices.

1. Introduction

Memcomputing, namely computing *with* and *in* memory, is a novel non-Turing paradigm of computation that employs memory elements to process and store information at the same physical location [1, 2]. Even though this paradigm could be realized with standard complementary metal-oxide-semiconductor (CMOS) technology [3], its main premises rest on the use of passive circuit elements with memory (memelements), namely, memristive, [4] memcapacitive and meminductive systems [5]. These memelements can indeed find numerous applications in electronics, including bio-inspired circuits, [6, 7] neuromorphic circuits [8, 9, 10] and various unconventional computing architectures [1, 11, 3, 12] – just to name a few.

Memcomputing can be employed in both analog and digital mode [1, 2] also combined with standard CMOS technology. [9, 13] The first mode of operation is ideal for the solution of optimization problems, otherwise difficult to solve using standard digital machines [2, 12, 14], as well as for analog computing [15]. Moreover, memristive [3, 16] and memcapacitive [17] neural networks can also be considered as an analog realization of memcomputing. The second – digital – mode combines the strengths of memcomputing (most notably its intrinsic massive parallelism) with standard digital logic functionality.

The possibility of performing logic operations directly in memory with memelements [11, 18, 1, 2, 19] could also solve the long-standing von Neumann bottleneck problem [20] of modern computer architectures. Since usual capacitors have practically very low dissipations, memcapacitive systems are ideal components to perform computation with little energy [21], thus offering a solution to another pressing problem in modern computers: the ever-increasing energy consumption of our digital machines [22].

In previous work we have suggested the use of solid-state memcapacitive systems with diverging and negative capacitance [23] to perform logic operations within an architecture inspired by the dynamic random access memory one. We called this architecture a Dynamic Computing Random Access Memory (DCRAM) [21]. It is worth noting, however, that although previously used solid-state memcapacitive systems can be used in digital mode, they are intrinsically analog elements. Memcapacitive systems that are fundamentally digital would thus be a better fit for this type of application although it is difficult to achieve 3D integration with membrane memcapacitors.

In this paper we employ the class of membrane memcapacitive systems [24] in the area of binary computing. Membrane memcapacitive systems (see a schematic in Fig. 1(a)) fit ideally in this context since stressed membranes have only two stable states unlike analog realizations of memcapacitive systems [25, 26, 23, 27]. The energy barrier between these two states plays the role of an intrinsic threshold that automatically assigns a binary value to any intermediate final state of the system. The combination of many of these membrane memcapacitive elements in an architecture like the DCRAM we have previously analyzed [21] would then represent an alternative way of implementing memcomputing in the solid state with passive devices. It is important to notice that

such systems can be realized using graphene membranes [28, 29, 30, 31] or any other molecular system as the flexible plate, and therefore our predictions are within reach of experimental verification.

There are several potential advantages of logic circuits based on membrane memcapacitive systems compared to traditional logic architectures. As mentioned above, the information processing and storage occur on the same physical platform. This feature reduces the amount of information transfer inside the computing system, bypassing altogether the data transfer between the memory and the central processing unit (CPU) where information is traditionally processed. In addition, it allows performing logic operations in memory in a massively-parallel and polymorphic way [21]. This latter feature means that the implementation of different logic functions is not based on any specific pre-wired structure. Rather, the type of logic operation is selected only by the control signal amplitudes. As such, memcapacitive logic circuits require much smaller number of individual components as well as offer a versatility inexistent in traditional logic circuits, even those employing memristive components [11].

2. Membrane memcapacitive system

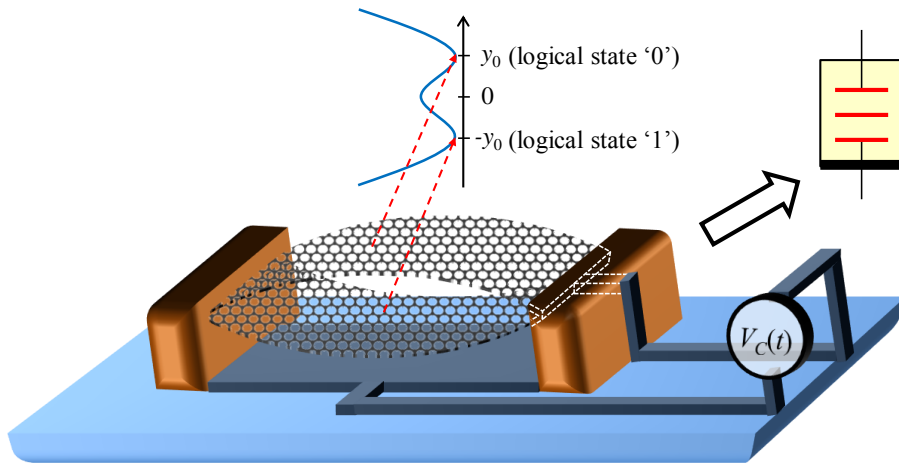


Figure 1. Schematics of membrane memcapacitive system and double well potential describing two equilibrium positions of the membrane at zero voltage.

By definition [5], a voltage-controlled memcapacitive system is given by the equations

$$q(t) = C(x, V_C, t) V_C(t) \quad (1)$$

$$\dot{x} = f(x, V_C, t) \quad (2)$$

where $q(t)$ is the charge on the capacitor at time t , $V_C(t)$ is the applied voltage, C is the *memcapacitance*, x is a set of n state variables describing the internal state

of the system, and f is a continuous n -dimensional vector function. It is important that the memcapacitance C depends on the state of the system and can vary in time. Some theoretical and experimental studies of memcapacitive effects can be found in the literature [25, 23, 26, 32, 33, 24, 27] (for a recent review, see Ref. [34]).

2.1. Membrane memcapacitor model

In the membrane memcapacitive system [24], the mechanism of memory capacitance is geometrical [34]. In this structure, the capacitor is formed by a strained membrane (upper plate) and a flat fixed lower plate as shown in Fig. 1. Two equilibrium states of flexible membrane (up-bent and down-bent) are suitable for non-volatile storage of bits of information. When the membrane is in a position closer to the bottom plate, the capacitance of the device is higher – we call this configuration '1'. When the membrane is bent up, the system has lower capacitance denoted by '0'.

A mathematical model of the membrane memcapacitive system formulated in Ref. [24] is based on a double-well potential (Fig. 1). This model describes the bistable membrane device as a second-order voltage-controlled memcapacitive system [5] in terms of the following equations:

$$q(t) = C(y)V_C(t), \quad (3)$$

$$\frac{dy}{d\tau} = \dot{y}, \quad (4)$$

$$\frac{d\dot{y}}{d\tau} = -4\pi^2 y \left(\left(\frac{y}{y_0} \right)^2 - 1 \right) - \Gamma \dot{y} - \left(\frac{\beta(\tau)}{1+y} \right)^2, \quad (5)$$

where

$$C(y) = \frac{C_0}{1+y}, \quad (6)$$

$y = z/d$, z is the position of the top membrane with respect to its middle position, d is the separation between the bottom plate and middle position of the flexible membrane, $y_0 = z_0/d$, $\Gamma = 2\pi\gamma/\omega_0$, $\beta(t) = 2\pi/(\omega_0 d) \sqrt{C_0/(2m)} V_C(t)$ and time derivatives are taken with respect to the dimensionless time $\tau = t\omega_0/(2\pi)$. Here, $\pm z_0$ are the equilibrium positions of the membrane, γ is the damping constant, ω_0 is the natural angular frequency of the system, m is the mass of the membrane and $C_0 = \epsilon_0 S/d$. The membrane displacement yd and membrane's velocity $\dot{y}d$ play the role of the internal state variables x_1 and x_2 (in Eqs. (1) and (2) $x = [x_1, x_2]$).

2.2. Membrane memcapacitor model including membrane resistance

An experimental realization of the bistable membrane memcapacitive system based on graphene was reported in Ref. [28]. It has been shown that the membrane dynamics can be described with a high precision by equations similar to Eqs. (4)-(5) at relatively large oscillation amplitudes ‡. At room temperatures, however, the

‡ Ref. [28] also reports a non-linear correction to the damping constant Γ proportional to $\sim y^2$ that appears at large oscillation amplitudes and is not really important for our consideration.

membrane resistance may become important (and it can also be modulated by doping the graphene sheets) [35, 36, 37]. Here we consider a modified model from Sec. 2.1 taking into account a finite membrane resistance R that is included in series with the membrane memcapacitance.

The external voltage $V(t)$ applied to the memcapacitive system is $V(t) = V_C(t) + V_R(t) = V_C(t) + RI(t)$, where $I(t) = dq(t)/dt$ is the current flowing through the memcapacitor. Eq. (3) must then be replaced by

$$q(t) = C(y)(V(t) - RI(t)). \quad (3a)$$

We define $\beta_0 = 2\pi/(\omega_0 d) \sqrt{C_0/(2m)}$, thus $\beta(t)$ in the the last term of Eq. (5) must be replaced by $\beta_0(V(t) - RI(t))$ and we can replace $I(t)$ by differentiating Eq. (3), i.e., $I(t) = d(C(y)V_C(t))/dt$. From these substitutions in the last term of Eq. (5) we obtain

$$\begin{aligned} \frac{dy}{d\tau} = & -4\pi^2 y \left(\left(\frac{y}{y_0} \right)^2 - 1 \right) - \left(\Gamma + \frac{\omega_0 \beta_0^2 RC_0}{\pi(1+y)^4} V(\tau) V_C(\tau) \right) \frac{dy}{d\tau} - \left(\frac{\beta_0 V(\tau)}{1+y} \right)^2 \times \\ & \times \left(1 - \frac{\omega_0 RC_0}{\pi V(\tau)(1+y)} \frac{dV_C(\tau)}{d\tau} \right) - \left(\frac{\omega_0 \beta_0 RC_0}{2\pi(1+y)^2} \right)^2 \left(\frac{dV_C(\tau)}{d\tau} - \frac{V_C(\tau)}{(1+y)} \frac{dy}{d\tau} \right)^2. \end{aligned} \quad (5a)$$

We note that in the case of nano-scale memcapacitors (for example with applications in VLSI circuits), both R and C_0 are very small, so we can safely neglect the terms in $(RC_0)^2$. Therefore, the above equation clearly shows that the resistance R increases the effective damping coefficient (i.e., the term multiplying dy/dt). In fact, the qualitative results from equations (3a) and (5a) are not different from these based on Eqs. (3) and (5). Therefore, for the sake of simplicity, only the simulation results based on the model without the resistance are presented below.

2.3. READ and WRITE operations

In order to perform logic functions, the circuit architecture should support single device READ/ WRITE operations as well as computing – the collective dynamics of coupled devices. This paper focuses on the computing functionality. Single device operations were considered in previous work [24]. The READ process involves a capacitance measurement, which can be performed by any suitable technique [38]. In particular, in our previous work [24] it was suggested to use differential voltage amplifiers (similar to those used in DRAMs) for reading purposes. The same technique could be employed to read the capacitance of the membrane memcapacitive systems. Charged to the same voltage, the smaller capacitance will result in a weaker current (below the threshold of the differential voltage amplifier) that could be distinguished from the stronger one (above the threshold).

Here, we just briefly review the more involved WRITE process. We note that in the presence of an applied voltage, the capacitor plates experience an attractive force toward each other. Correspondingly, the double well potential from Fig. 1 becomes asymmetric

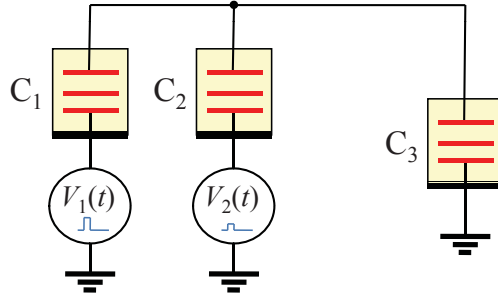


Figure 2. Circuit considered in this work. Here, memcapacitive systems C_1 and C_2 hold input values, while C_3 the output one. Two voltage sources are used to subject the input memcapacitive systems C_1 and C_2 to pulse sequences $V_1(t)$ and $V_2(t)$.

– its right minimum moves up while the left one moves down. At a certain voltage magnitude, the right minimum disappears and the system, regardless of its initial state, ends up in the left minimum. This is the basis to set the system to '1'. In order to set the system to '0', a higher voltage is needed. When such voltage is applied and then removed, an accumulated elastic energy becomes sufficiently strong to overcome the potential barrier and set the system to '0' (see Ref. [24] for more details).

3. Logic gate

We consider first logic operations with the circuit shown in Fig. 2. This circuit involves three memcapacitive systems and two voltage sources and can be considered as a sub-part of a larger circuit, effectively decoupled from this larger circuit with appropriate switches. Such a larger circuit could be, for example, similar to the DCRAM architecture we have previously introduced [21]. In fact, like in our previous work [21] with solid-state memcapacitive systems [23], we expect more cells will provide a larger set of logic gates at different voltages.

For the sake of simplicity, we do not show any initialization and measurement setup in Fig. 2 since only the computing stage is of interest. All results reported in this paper were obtained utilizing completely overlapping single square pulses $V_1(t)$ and $V_2(t)$, as shown in the top panel of Fig. 3.

The circuit dynamics is found using Kirchhoff's circuit laws together with Eqs. (3)-(5) defining the response and dynamics of memcapacitive devices. In particular, one can find that at each moment of time the voltages across the three memcapacitive systems are given by

$$V_{C_1} = \frac{C_2 V_2(t) - (C_2 + C_3) V_1(t)}{C_1 + C_2 + C_3}, \quad (7)$$

$$V_{C_2} = \frac{C_1 V_1(t) - (C_1 + C_3) V_2(t)}{C_1 + C_2 + C_3}, \quad (8)$$

$$V_{C_3} = \frac{C_1 V_1(t) + C_2 V_2(t)}{C_1 + C_2 + C_3}, \quad (9)$$

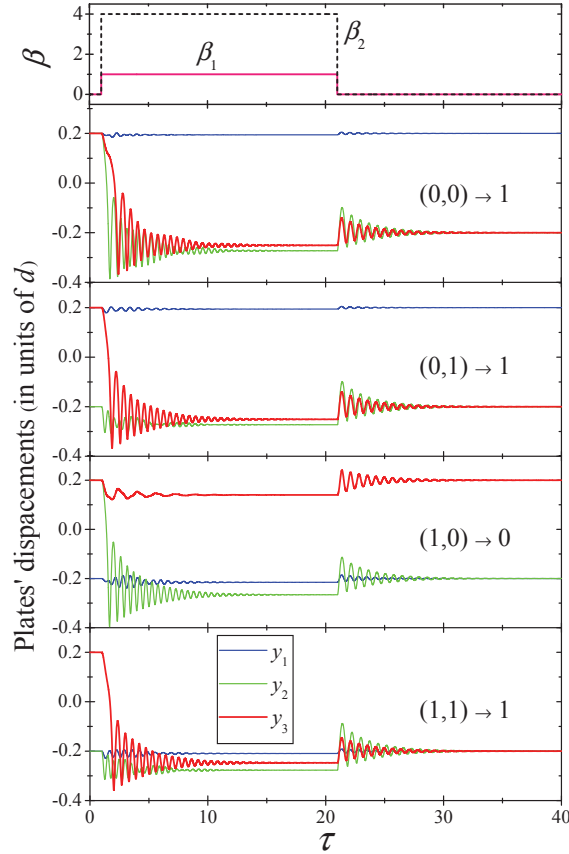


Figure 3. Material implication $(C_1 \rightarrow C_2) = C_3$ with membrane memcapacitive systems. The four bottom plots show dynamics of coupled memcapacitive systems (according to Fig. 2 circuit configuration) at different initial conditions. The voltage pulses are demonstrated in the top plot. The initial state of C_3 is always '0'. These plots were obtained using the parameter values $\Gamma = 0.7$ and $y_0 = 0.2$.

where the voltages are defined with respect to the terminal denoted by the thick line in the memcapacitive system symbol in Fig. 2. These instantaneous values of voltages influence the dynamics of the internal state variables through Eq. 5. In what follows, it is assumed that the input values are stored in C_1 and C_2 , while C_3 is reserved for the output value. However, for certain regions of pulse parameters, the final states of C_1 and C_2 are different from the input ones. Therefore, these two memcapacitive systems could also be used to store the computing result in some cases and thus few different logic operations could be realized in a single shot (see also Sec. “Reduced circuit”).

3.1. Material implication

We are now ready to show that these membrane memcapacitive systems are able to perform logic operations. To do this we focus on the logic material implication previously demonstrated with memory resistive devices [11]. Material implication is a very important logic function because it can be used to synthesize the negation (with

Table 1. Codes of certain logic operations calculated according to Eq. (10). These codes are defined with respect to different pairs of input values (C_1, C_2). For example, NOT C_1 is the logical negation on C_1 , copy C_2 is the copy of the input state of C_2 into the final state of a given system, IMP_1 is the material implication $C_1 \rightarrow C_2$, etc. More details are given in the text.

set to 0	0	AND	8
NOR	1	NOT(XOR)	9
NOT(IMP_2)	2	copy C_2	10
NOT C_1	3	IMP_1	11
NOT(IMP_1)	4	copy C_1	12
NOT C_2	5	IMP_2	13
XOR	6	OR	14
NAND	7	set to 1	15

the help of a false operation), which, together with implication, allows for a functionally complete set of logic gates.

In order to demonstrate the material implication, let us consider the circuit dynamics at specific amplitudes of voltage pulses $\beta_1(\tau)$ and $\beta_2(\tau)$, namely, $\beta_1 = 1$ and $\beta_2 = 4$. Fig. 3 shows the dynamics of the internal states of memcapacitive systems (the position of the flexible plate) for four possible initial states of C_1 and C_2 . It is assumed that C_3 is in '0' state at $\tau = 0$. Clearly, C_3 remains in '0' only at the (1,0) input combination and its final state is '1' for all other input combinations. This is the material implication. We also note that the final state of C_2 is always '1'. The state of C_1 remains unchanged during the circuit dynamics operation.

3.2. Map of logic operations

In order to better understand which logic operations can be implemented with the memcapacitive logic circuit from Fig. 2, we prescribe a numerical value to operation results as follows. Taking $w_i = 1, 2, 4, 8$ as weights for the input combinations (0,0), (0,1), (1,0) and (1,1), a numerical code is calculated as a weighted sum of the final state of a particular memcapacitive system, namely,

$$\text{code} = \sum_{i=1}^4 w_i b_{ij}^f, \quad (10)$$

where b_{ij}^f is the final state (0 or 1) of the device of interest j (C_1, C_2 or C_3) for i -th input combination (0,0), (0,1), (1,0) or (1,1) that correspond to $i = 1, 2, 3, 4$. For example, for the material implication function shown in Fig. 3, the code for the final state of C_3 is $1 \cdot 1 + 2 \cdot 1 + 4 \cdot 0 + 8 \cdot 1 = 11$. Therefore, 11 is the code for material implication $C_1 \rightarrow C_2$.

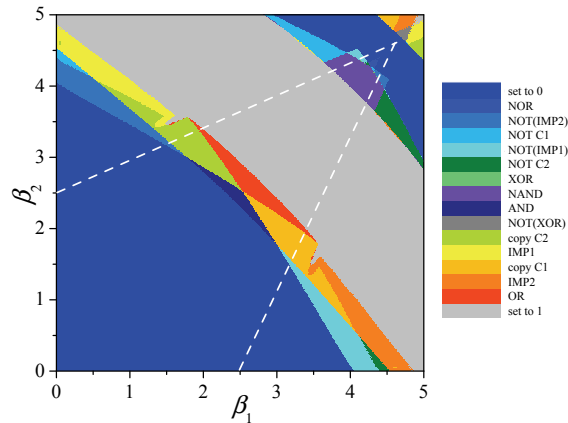


Figure 4. Logic operation type as a function of pulse amplitudes β_1 and β_2 for the output memcapacitive system C_3 . Each point of this plot was obtained with a calculation similar to that shown in Fig. 3. This plot was obtained using the pulse width $T = 20$, $\Gamma = 0.7$, $y_0 = 0.2$. The region between two white dashed lines corresponds approximately to the operation regime such that C_1 and C_2 stay unchanged.

Similarly, one can find that the material implication $C_2 \rightarrow C_1$ corresponds to the code value 13. Table 1 summarizes the codes for all operations implemented with membrane memcapacitive logic.

Fig. 4 is the main result of this work. It identifies the regions of voltage pulse amplitudes β_1 and β_2 realizing specific logic functions as the final state of C_3 . Each point of this plot is calculated similarly to Sec. “Material implication” calculation assuming that C_3 is in 0 at $t = 0$. As expected, at smaller values of β_1 or β_2 and any input combination, the final state of C_3 is 0. Material implication, OR, NAND and some other functions are found at higher values of the applied pulses as shown in Fig. 4. This calculation demonstrates that the same memcapacitive circuit is capable of realizing different logic functions on demand without any changes in the circuit configuration. The circuit thus performs *polymorphic* computing in the sense discussed in Ref. [21].

The final states of C_1 and C_2 are shown in Fig. 5. Although there are large regions where C_1 and C_2 stay unchanged, one can identify regions of amplitudes implementing the material implication (codes 11 and 13), ‘set to 1’ (code 15) and some other functions. Therefore, a logic function and initialization or two different logic functions can be performed in a single step (intrinsic parallelism [1, 2]) thus further increasing the efficiency of calculations.

We also note that there are regions in the input-voltage parameter phase space that show non-trivial features such as those two irregularities observed at approximately $(\beta_1 = 1.5, \beta_2 = 3.5)$ and $(\beta_1 = 3.5, \beta_2 = 1.5)$ in Fig. 4. Figure 6 shows the feature magnification revealing additional fine structures (straight lines) in those regions. These features originate from the complex dynamics of memcapacitive systems already spotted in a previous work of one of us [24]. We emphasize that such irregularities are observed only in limited intervals of voltage amplitudes, and therefore can be easily avoided

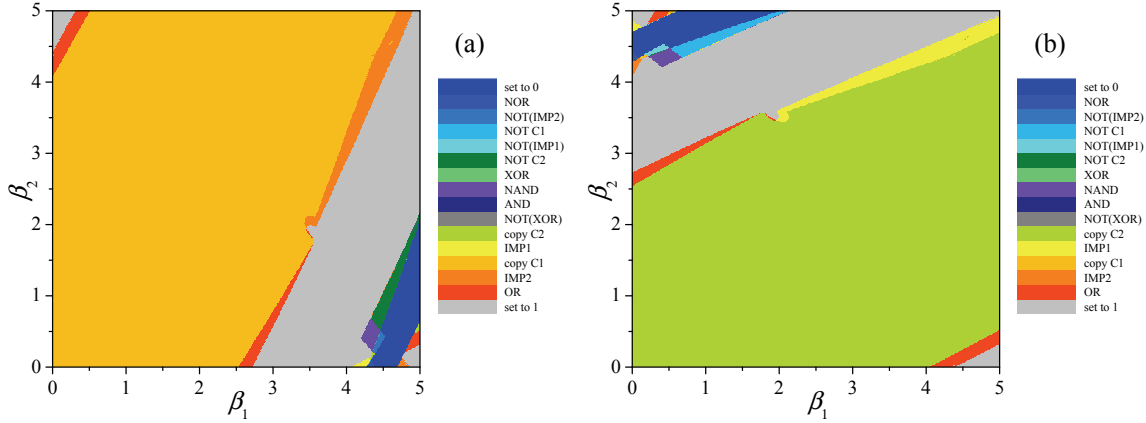


Figure 5. Logic operation type as a function of pulse amplitudes β_1 and β_2 for the input memcapacitive systems C_1 , (a), and C_2 , (b). The data for these plots and Fig. 4 were obtained within the same calculations.

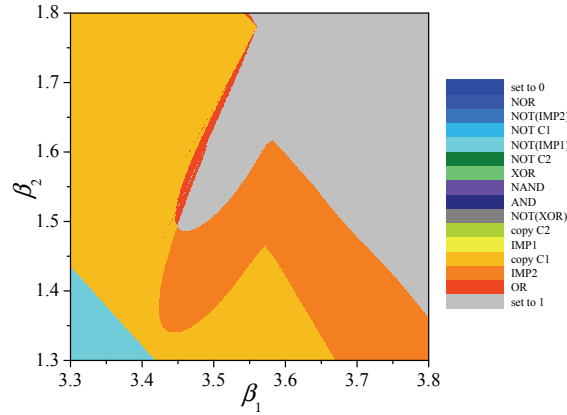


Figure 6. Magnified region of Fig. 4 showing non-trivial fine structures.

in practical realizations of membrane memcapacitive systems. Moreover, by varying geometrical (y_0) and physical (Γ) parameters as shown in the Supporting Information, the chaotic behavior of the circuit can be minimized.

3.3. Reduced circuit

The results presented in Fig. 5 demonstrate that the same memcapacitive device could store both input and output logic values. In order to better understand this capability we consider a reduced circuit consisting of two memcapacitive systems as sketched in Fig. 7(a). We have performed simulations of the circuit dynamics subjected to the same couple of pulses and simulation parameters as we have discussed above.

The results of these simulations presented in Fig. 7(b) demonstrate that even such a simple circuit is capable of implementing the OR gate in a significant interval of parameters. However, a single OR is not enough for universal computing. One

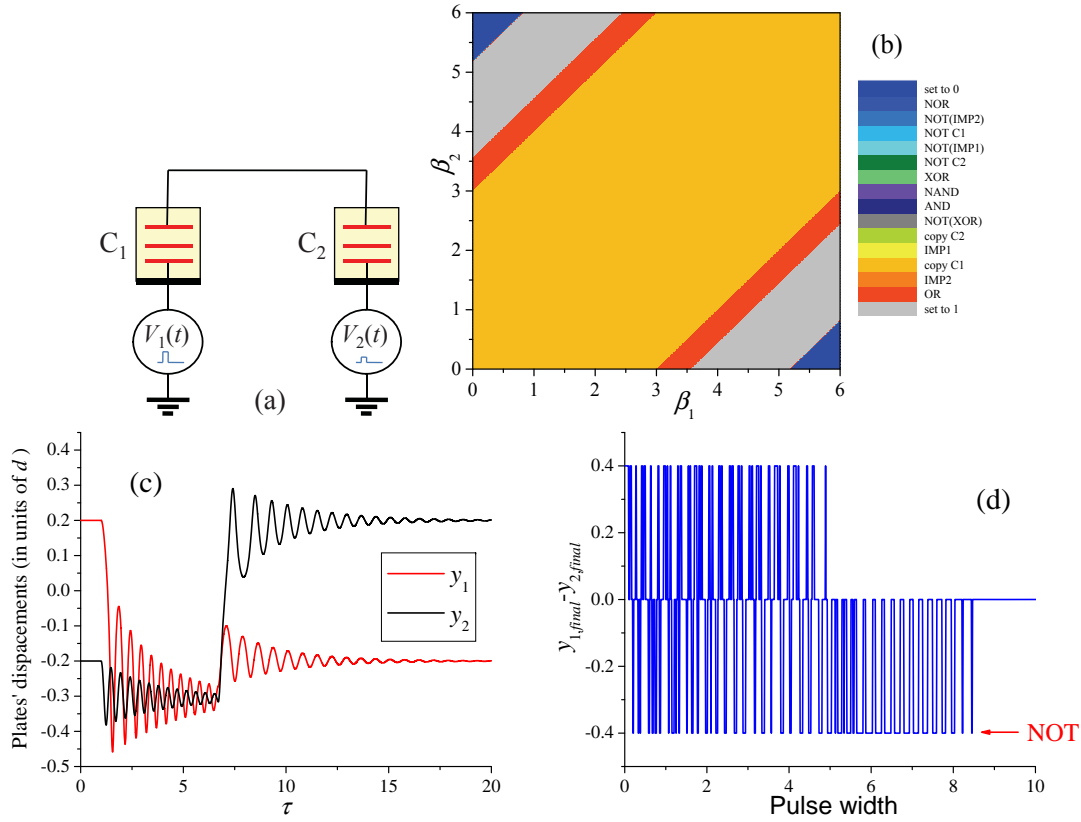


Figure 7. (a) Reduced circuit layout. (b) Logic operation type as a function of pulse amplitudes β_1 and β_2 calculated for the final state of C_1 . (c) Demonstration of the NOT gate with a single memcapacitive system: $0 \rightarrow 1$ and $1 \rightarrow 0$ when the system is subjected to the same pulse of $\beta = 2.8$ magnitude and $T = 5.7$ duration. (d) Final $y_1 - y_2$ as a function of the pulse width at the same value of $\beta = 2.8$ showing intervals of the NOT gate.

possibility to attain this goal would be a combination of the OR gate and NOT gates. Considering dynamics of a single membrane memcapacitive system subjected to a voltage pulse, we have indeed found pulse parameters realizing the NOT. Fig. 7(c) shows an example of such realization.

In order to better understand the NOT implementation, we plot the difference of final positions of plates for different initial conditions ($y_1(0) = 0.2$ and $y_2(0) = -0.2$), namely, $y_1 - y_2$ at $\tau = 40$. The NOT is realized when $y_1(40) = -0.2$ and $y_2(40) = 0.2$. In other words, when the final $y_1 - y_2 = -0.4$. Fig. 7(d) shows multiple regions of the NOT gate, which could be achieved, for the set of system parameters selected, using a fine pulse width tuning. We emphasize that a further improvement of membrane memcapacitive logic is possible. For example, a larger set of logic operations with two memcapacitive devices could possibly be obtained adding a capacitor to the circuit in Fig. 7(a). A pulse engineering is an additional opportunity that could lead to improved functionality.

4. Impact of Device Parameters

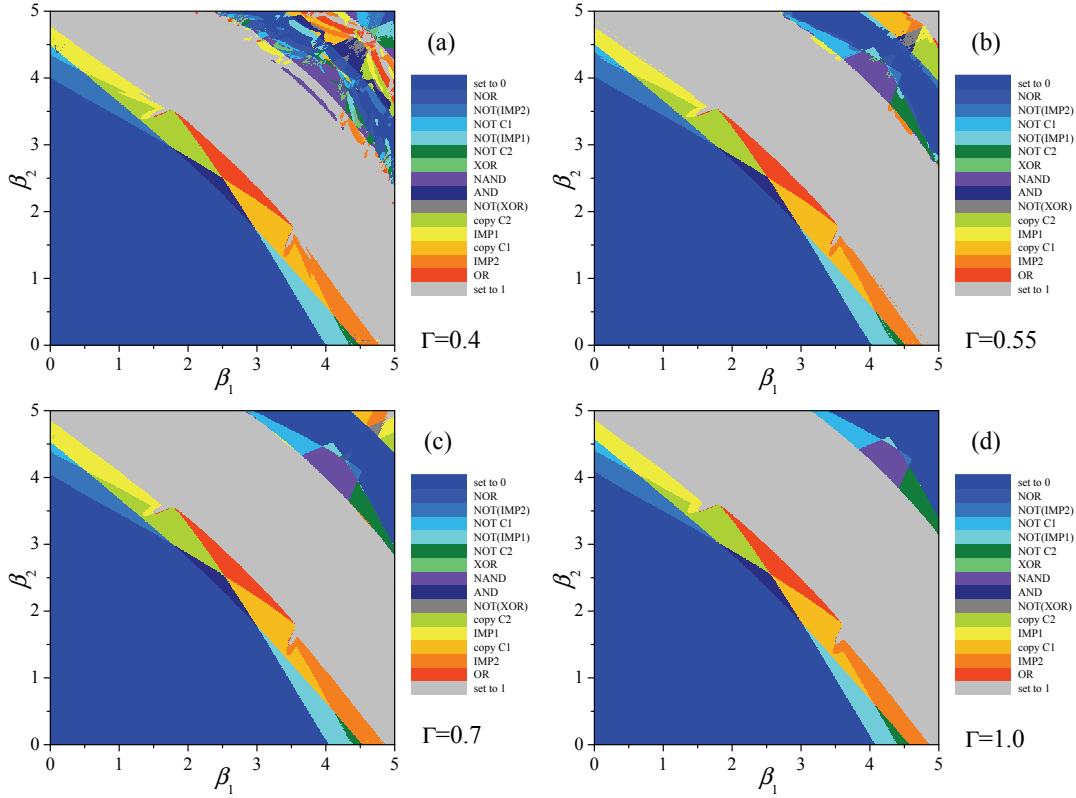


Figure 8. Logic operation type as a function of pulse amplitudes β_1 and β_2 for the output memcapacitive system C_3 for $y_0 = 0.2$ and several values of parameter Γ as indicated. The calculations were performed for the circuit configuration shown in Fig. 2 assuming two completely overlapping applied pulses of $T = 20$ width.

In order to better understand the implementation of logic operations with membrane memcapacitive systems, we have performed several additional calculations varying parameters y_0 and Γ of the model. Figure 8 shows results of these calculations for a circuit of three memcapacitive systems (depicted in Fig. 2) at a fixed value of $y_0 = 0.2$ and several representative values of Γ . This figure demonstrates that at smaller values of Γ (Fig. 8(a) and (b)) there is a significant region of chaotic-like behavior at larger values of β_1 and β_2 (see the top right parts of these plots). Increasing Γ stabilizes this region (Fig. 8(c) and (d)). Clearly, already at $\Gamma = 0.7$ there are no hints of uncertainty in that large β_1 and β_2 region. Therefore, while the chaotic-like behavior is already not possible at $\Gamma = 0.7$, a larger value of Γ could be used in experimental realizations of the circuit to guarantee its operation stability.

Figure 9 shows the results of simulations for the same three-device circuit (Fig. 2) at a fixed value of $\Gamma = 0.7$ and several values of y_0 . It follows from Fig. 9 that the regions of useful logic functions are significantly increased with increasing y_0 . There are three potentially interesting regions in Fig. 9(d) (codes 7, 11, 13) corresponding

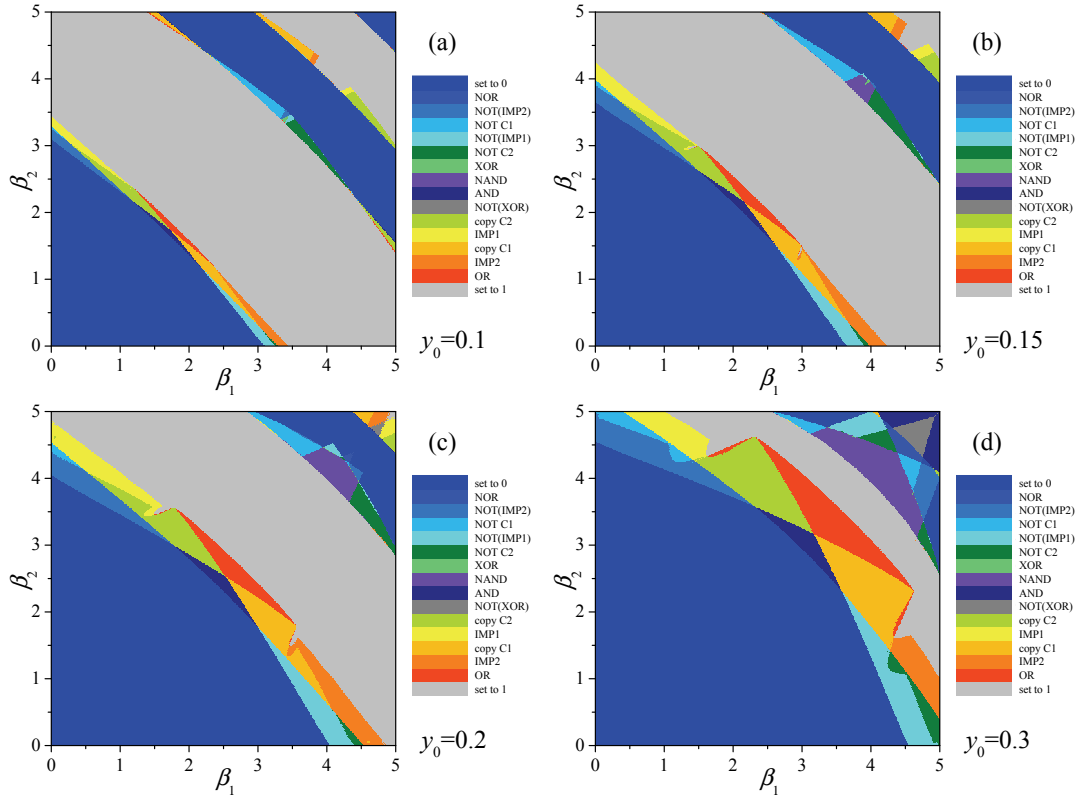


Figure 9. Logic operation type as a function of pulse amplitudes β_1 and β_2 for the output memcapacitive system C_3 for $\Gamma_0 = 0.2$ and several values of parameter y_0 as indicated. The calculations were performed for the circuit configuration shown in Fig. 2 assuming two completely overlapping applied pulses of $T = 20$ width.

to NAND and material implications. Each of these regions provides a universal logic capability.

5. Conclusions

We have shown that memcomputing—computing *with* and *in* memory— [1] can be implemented with membrane memcapacitive systems. This demonstrates that this quite different type of memcapacitive system (compared to the solid-state memcapacitive systems previously studied [21]) is also suitable for massively parallel and polymorphic computing operations directly in memory, thus offering a different realization of the memcomputing concept. Experimentally, our predictions could be verified with membrane memcapacitive systems employing, e.g., a stressed graphene membrane \S , a synthetic (artificial) membrane, or a molecular system as the flexible plate. Graphene membranes, for instance, have been recently demonstrated experimentally as systems for quantum information [31]. Here, instead we suggest their use as semi-classical two-level systems. We thus hope our predictions will motivate further experimental and

\S Graphene is currently used in experimental capacitors [28, 29, 30] albeit in a different role.

theoretical work in this direction.

From the fabrication point of view, the membrane memcapacitive memory could be realised in a CMOL-like architecture [39], which is a hybrid architecture combining a semiconductor-transistor (CMOS) layer with a layer of molecular-scale nanodevices formed between two levels of parallel nanowires [39]. In our case, the top layer will be a layer of membrane memcapacitive systems coupled with the bottom CMOS layer using a set of vertical connections. It is anticipated that a single graphene-based memcapacitive system could be scaled down to few 100s nm² area. The amount of memcapacitive systems scales almost linearly with the chip area and the most natural architecture to include circuitry to control computing, reading and writing processes is the well scalable DRAM-like architecture [21]. Furthermore, membrane memcapacitive systems are passive systems (excluding control circuitry) thus the energy per operation can be as small as the energy required for the voltage pulses used to read/write and compute, that is typically of the order of few fJ for standard technologies [21]. Finally, the maximum operation frequency (being passive) is directly related to the membrane damping constant γ , thus strongly depending on the materials and technologies used to build the memcapacitors, for example, how the membrane is attached to the substrate strongly affects γ . For example, from Ref. [28] and from some rough estimation, a working frequency could be of the order of a hundred MHz. However, in this case very large sheets of graphene have been used and the temperature is very low. We think that at higher temperatures (where the sheet resistance is higher, see section 2.2 for the impact of the resistance on the effective damping parameter) and much smaller membrane sizes, a working frequency of at least few GHz can be reached.

6. Acknowledgment

This work has been partially supported by the NSF grant ECCS-1202383, and the Center for Magnetic Recording Research at UCSD.

References

- [1] Massimiliano Di Ventra and Yuriy V. Pershin. The parallel approach. *Nature Physics*, 9:200, 2013.
- [2] F.L. Traversa and M. Di Ventra. Universal memcomputing machines. *IEEE Trans. Neural Netw. Learn. Syst.*, (DOI: 10.1109/TNNLS.2015.2391182, preprint arXiv:1405.0931), 2015.
- [3] Yuriy V. Pershin and Massimiliano Di Ventra. Experimental demonstration of associative memory with memristive neural networks. *Neural Networks*, 23:881, 2010.
- [4] Leon O. Chua and Sung Mo Kang. Memristive devices and systems. *Proc. IEEE*, 64:209–223, 1976.
- [5] Massimiliano Di Ventra, Yuriy V. Pershin, and Leon O. Chua. Circuit elements with memory: Memristors, memcapacitors, and meminductors. *Proc. IEEE*, 97(10):1717–1724, 2009.
- [6] Y. V. Pershin, S. La Fontaine, and M. Di Ventra. Memristive model of amoeba learning. *Phys. Rev. E*, 80:021926, 2009.
- [7] F. L. Traversa, Y. V. Pershin, and M. Di Ventra. Memory models of adaptive behaviour. *IEEE Trans. Neural Netw. Learn. Syst.*, 24:1437 – 1448, 2013.

- [8] Sung Hyun Jo, Ting Chang, Idongesit Ebong, Bhavitavya B. Bhadviya, Pinaki Mazumder, and Wei Lu. Nanoscale memristor device as synapse in neuromorphic systems. *Nano Lett.*, 10:1297–1301, 2010.
- [9] Kuk-Hwan Kim, Siddharth Gaba, Dana Wheeler, Jose M. Cruz-Albrecht, Tahir Hussain, Narayan Srinivasa, and Wei Lu. A functional hybrid memristor crossbar-array/cmos system for data storage and neuromorphic applications. *Nano Letters*, 12(1):389–395, 2012.
- [10] Y. V. Pershin and M. Di Ventra. Neuromorphic, digital and quantum computation with memory circuit elements. *Proc. IEEE*, 100:2071, 2012.
- [11] Julien Borghetti, Gregory S. Snider, Philip J. Kuekes, J. Joshua Yang, Duncan R. Stewart, and R. Stanley Williams. ‘Memristive’ switches enable ‘stateful’ logic operations via material implication. *Nature*, 464:873–876, 2010.
- [12] Yuriy V. Pershin and Massimiliano Di Ventra. Solving mazes with memristors: a massively-parallel approach. *Phys. Rev. E*, 84:046703, 2011.
- [13] Qiangfei Xia, Warren Robinett, Michael W. Cumbie, Neel Banerjee, Thomas J. Cardinali, J. Joshua Yang, Wei Wu, Xuema Li, William M. Tong, Dmitri B. Strukov, Gregory S. Snider, Gilberto Medeiros-Ribeiro, and R. Stanley Williams. Memristor-CMOS hybrid integrated circuits for reconfigurable logic. *Nano Letters*, 9:3640–3645, 2009.
- [14] Yuriy V. Pershin and Massimiliano Di Ventra. Self-organization and solution of shortest-path optimization problems with memristive networks. *Phys. Rev. E*, 88:013305, Jul 2013.
- [15] C. David Wright, Yanwei Liu, Krisztian I. Kohary, Mustafa M. Aziz, and Robert J. Hicken. Arithmetic and biologically-inspired computing using phase-change materials. *Advanced Materials*, 23:3408–3413, 2011.
- [16] Andy Thomas. Memristor-based neural networks. *Journal of Physics D: Applied Physics*, 46(9):093001, 2013.
- [17] Yuriy V. Pershin and Massimiliano Di Ventra. Memcapacitive neural networks. *Electronics Letters*, 50:141, 2014.
- [18] E Linn, R Rosezin, S Tappertzhofen, U Böttger, and R Waser. Beyond von Neumann-logic operations in passive crossbar arrays alongside memory operations. *Nanotechnology*, 23(30):305205, 2012.
- [19] A. V. Ievlev, S. Jesse, A. N. Morozovska, E. Strelcov, E. A. Eliseev, Y. V. Pershin, A. Kumar, V. Ya. Shur, and S. V. Kalinin. Intermittency, quasiperiodicity and chaos in probe-induced ferroelectric domain switching. *Nature Physics*, 10:59–66, 2014.
- [20] J. Backus. Can programming be liberated from the von Neumann style? a functional style and its algebra of programs. *Comm. ACM*, 21:613–641, 1978.
- [21] F. L. Traversa, F. Bonani, Y. V. Pershin, and M. Di Ventra. Dynamic computing random access memory. *Nanotechnology*, 25:285201, 2014.
- [22] P. Kogge. The tops in flops. *IEEE Spectrum*, 48:48–54, 2011.
- [23] J. Martinez-Rincon, Massimiliano Di Ventra, and Yuriy V. Pershin. Solid-state memcapacitive system with negative and diverging capacitance. *Phys. Rev. B*, 81:195430, 2010.
- [24] J. Martinez-Rincon and Yuriy V. Pershin. Bistable non-volatile elastic membrane memcapacitor exhibiting chaotic behavior. *IEEE Trans. El. Dev.*, 58:1809, 2011.
- [25] Shangqing Liu, Naijuan Wu, Alex Ignatiev, and Jianren Li. Electric-pulse-induced capacitance change effect in perovskite oxide thin films. *J. Appl. Phys.*, 100:056101, 2006.
- [26] Qianxi Lai, Lei Zhang, Zhiyong Li, William F. Stickle, R. Stanley Williams, and Yong Chen. Analog memory capacitor based on field-configurable ion-doped polymers. *Appl. Phys. Lett.*, 95:213503, 2009.
- [27] J Flak, E Lehtonen, M Laiho, A Rantala, M Prunnila, and T Haatainen. Solid-state memcapacitive device based on memristive switch. *Semiconductor Science and Technology*, 29(10):104012, 2014.
- [28] A. Eichler, Joel Moser, J. Chaste, M. Zdrojek, I. Wilson-Rae, and Adrian Bachtold. Nonlinear damping in mechanical resonators made from carbon nanotubes and graphene. *Nature nanotechnology*, 6(6):339–342, 2011.

- [29] Meryl D. Stoller, Sungjin Park, Yanwu Zhu, Jinho An, and Rodney S. Ruoff. Graphene-based ultracapacitors. *Nano Letters*, 8(10):3498–3502, 2008.
- [30] Maher F. El-Kady and Richard B. Kaner. Scalable fabrication of high-power graphene micro-supercapacitors for flexible and on-chip energy storage. *Nature Communications*, 4:1475, 2013.
- [31] V. Singh, S. J. Bosman, B. H. Schneider, Y. M. Blanter, Castellanos-Gomez A., and G. A. Steele. Optomechanical coupling between a multilayer graphene mechanical resonator and a superconducting microwave cavity. *Nature Nanotechnology (advanced online publication)*, 2014.
- [32] D. Biolek, Z. Biolek, and V. Biolkova. SPICE modelling of memcapacitor. *El. Lett.*, 46:520, 2010.
- [33] Matt Kreams, Yuriy V. Pershin, and Massimiliano Di Ventra. Ionic memcapacitive effects in nanopores. *Nano Lett.*, 10:2674, 2010.
- [34] Yuriy V. Pershin and Massimiliano Di Ventra. Memory effects in complex materials and nanoscale systems. *Advances in Physics*, 60:145–227, 2011.
- [35] Sukanta De and Jonathan N. Coleman. Are there fundamental limitations on the sheet resistance and transmittance of thin graphene films? *ACS Nano*, 4(5):2713–2720, 2010. PMID: 20384321.
- [36] Ki Kang Kim, Alfonso Reina, Yumeng Shi, Hyesung Park, Lain-Jong Li, Young Hee Lee, and Jing Kong. Enhancing the conductivity of transparent graphene films via doping. *Nanotechnology*, 21(28):285205, 2010.
- [37] Hongtao Liu, Yunqi Liu, and Daoben Zhu. Chemical doping of graphene. *J. Mater. Chem.*, 21:3335–3345, 2011.
- [38] V.P. Petkov and B.E. Boser. Capacitive interfaces for mems. In H. Baltes, O. Brand, G. K. Fedder, C. Hierold, J. G. Korvink, and O. Tabata, editors, *Advanced Micro and Nanosystems*, pages 49–92. Wiley-VCH, Weinheim, Weinheim, 2004.
- [39] DB Strukov and KK Likharev. CMOL FPGA: a reconfigurable architecture for hybrid digital circuits with two-terminal nanodevices. *Nanotechn.*, 16:888–900, 2005.